Article:
Bonakdar, T, Ali, M and Ghadiri, M orcid.org/0000-0003-0479-2845 (2021) Particle breakability assessment using an Aero S disperser. International Journal of Pharmaceutics, 597. 120365. ISSN 0378-5173

https://doi.org/10.1016/j.ijpharm.2021.120365

PARTICLE BREAKABILITY ASSESSMENT USING AN AERO S DISPERSER

Tina Bonakdar[1], Muzammil Ali[2] and Mojtaba Ghadiri[*]

**School of Chemical and Process Science and Engineering, University of Leeds, Leeds LS2 9JT, UK*

ABSTRACT

Milling is widely used in various industries to tailor the particle size distribution for desired attributes. The ability to predict milling behaviour by testing the breakability of a small quantity of material is of great interest. In this paper, a widely available aerodynamic dispersion method, i.e. the Aero S disperser of Malvern Mastersizer 3000 has been evaluated for this purpose. This device is commonly used for dispersion of fine and cohesive powders, as the particles are accelerated and impacted at a bend, but here its use for assessing particle breakability is explored. The fluid flow field is modelled using one-way coupled Computational Fluid Dynamics approach, as the particle concentration is low, following which the particle impact velocity is calculated by Lagrangian tracking and used in the analysis of particle breakage. Experimental work on the breakability is carried out using aspirin, paracetamol, sucrose and α–lactose monohydrate particles. The relative shift in the specific surface area is determined and together with the calculated particle impact velocity and physical properties, they are used to calculate the breakability index. A good agreement is obtained with the single particle impact testing and aerodynamic dispersion by Scirocco disperser, indicating the breakability could also be inferred from this method.

Keyword: Aero S, impact, breakage, dispersion, size reduction, milling, grinding

1. INTRODUCTION

Particle size reduction is widely carried out in various industries, including pharmaceutical, food, chemical and mineral to impart desired material attributes, such as good dissolution, ability to prepare strong tablets and compacts, or getting the right taste or colour. At the early stages of product development, particularly in the pharmaceutical industry, there is quite often a very small amount of material available for testing for process development. So

[1] Current address: Pfizer Ltd, Ramsgate Road, Sandwich CT13 9NJ, UK
[2] Current address: Fluid Comp Limited, Leeds, LS6 1RD, UK

development of predictive ability based on the smallest possible sample quantity is of great interest.

Breakage testing by impact has been well established and it is particularly suitable for materials that are strain rate sensitive, because quasi-static crushing could cause extensive plastic deformation and hence the breakage trend may not correlate with milling operations. There are a number of factors influencing particle breakage under impact stressing conditions, such as particle size, shape and density, mechanical properties, pre-exiting flaws, impact velocity and angle as well as the number of impacts. The breakage characteristics of different materials in stirred media mills and their relation with the stress intensity and frequency of stressing events have been analysed by Kwade and Schwedes (2002). As shown by Vogel and Peukert (2003) for brittle failure and by Ghadiri and Zhang (2002) for semi-brittle failure, the breakage probability in the case of the former and the extent of breakage for the latter are directly proportional to the particle size. Regarding the effect of impact velocity, the functional dependence of the extent of breakage on impact velocity depends on the mechanical and physical properties, but in general it scales with the incident kinetic energy. For the brittle failure mode, the breakage is rather insensitive to the strain rate, and usually quasi-static and dynamic impact stressing produce comparable tensile stress fields (Shipway and Hutchings, 1993). Nevertheless at very high strain rates, elastic wave propagation influences particle breakage, as shown by Gong et al (2018). In contrast, in the case of semi-brittle failure, there is notable sensitivity to strain-rate hardening, due to dislocation mobility constraints (Chaudhri *et al*., 1981) and impact stressing promotes cleavage fracture, if present, as compared to dislocation glide on slip planes in quasi-static stressing (Olusanmi *et al.*, 2011). Moreover, particle strength depends on its production history, whether it has been generated as a result of larger particles breaking into the size (Petukhov and Kalman, 2004) or grown by crystallization (Meier et al., 2009) or agglomeration (Salman *et al*., 2002 & 2004). For brittle failure, it is the size, number density and position of flaws that determine the strength, and particle breakage is well described by Weibull analysis (Vogel and Peukert, 2003), whilst for the semi-brittle failure stiffness, hardness and toughness are accountable for crack initiation and propagation (Meier et al., 2009 and Ghadiri et al., 2020).

A number of apparatuses have been developed and used for impact testing, but are not commercially available; examples are the single particle impact testers (Yüregir *et al.*, 1986; Lecoq *et al.*, 2003 and 2011; Salman *et al.*, 2002; Petukhov and Kalman, 2003), drop weight testers based on Schönert's design (Schönert and Marktscheffel, 1986; Vogel and Peukert,

2003; Meier *et al.*, 2008), ultrafast load cell (Weichert and Herbst, 1986), impact load cell (Tavares, 1998; Saeidi *et al.*, 2017). In contrast, there are aerodynamic dispersion units, which have been developed for particle size analysis and are widely available in particle technology laboratories, e.g. the Scirocco disperser of Mastersizer 2000 and the Aero S disperser of Mastersizer 3000 (both of Malvern Panalytical), Rodos of Sympatec, Partica of Horiba. The particle breakability using the Scirocco disperser of Malvern Mastersizer 2000 has previously been evaluated by Ali *et al.* (2015). The work has highlighted the potential of using this device and a method for impact breakage test to assess the grindability of materials. Bonakdar *et al.* (2016) used the Scirocco disperser to evaluate the breakability of the same materials as used here. Fulchini *et al.* (2017) also used the same technique to evaluate the attrition propensity of Chemical Looping Catalyst, where the particulate solids circulate between two fluidised beds, in which the solids undergo alternate chemical oxidation to chemical reduction and experience attrition. Bonakdar and Ghadiri (2018) used the breakage kernels obtained by the Scirocco disperser to predict the size reduction of pharmaceutical materials in a pin mill.

In this work the breakability testing using the Aero S dispersion unit of Malvern Mastersizer 3000 is addressed. Particles are accelerated by a high velocity air jet in a Venturi arrangement. There are in fact two setup arrangements, one for free flowing powders and grains for which the particles are immediately introduced to the laser diffraction unit for sizing following a straight section after the Venturi. The other setup, as shown in Figure 1, has been devised for dispersing cohesive powders, where the presence of a 90° elbow helps disintegrating and dispersing cohesive clusters before sizing by the laser diffraction unit (Calvert *et al.*, 2009). For accurate sizing of the feed particles, care should in fact be taken by using the right dispersion condition so as not to cause damage to the feed particles (Hebbink and Dickhoff, 2019), but at the same time ensure full dispersion. However, here the latter setup has been used to deliberately impart impact damage to the particles so as to assess their breakability. Damaged particles are presented immediately to the laser diffraction unit for sizing. This approach is suitable for particles which undergo chipping and fragmentation upon impact on the bend of the unit. The high-pressure air is supplied at inlet port 1, connected internally to a nozzle which produces a high velocity air jet and slight vacuum, thereby entraining particles (port 2) towards the high velocity jet. The particles are accelerated with the air flow in the jet and impact at the elbow, potentially causing breakage at sufficiently high velocity, then leaving via port 3.

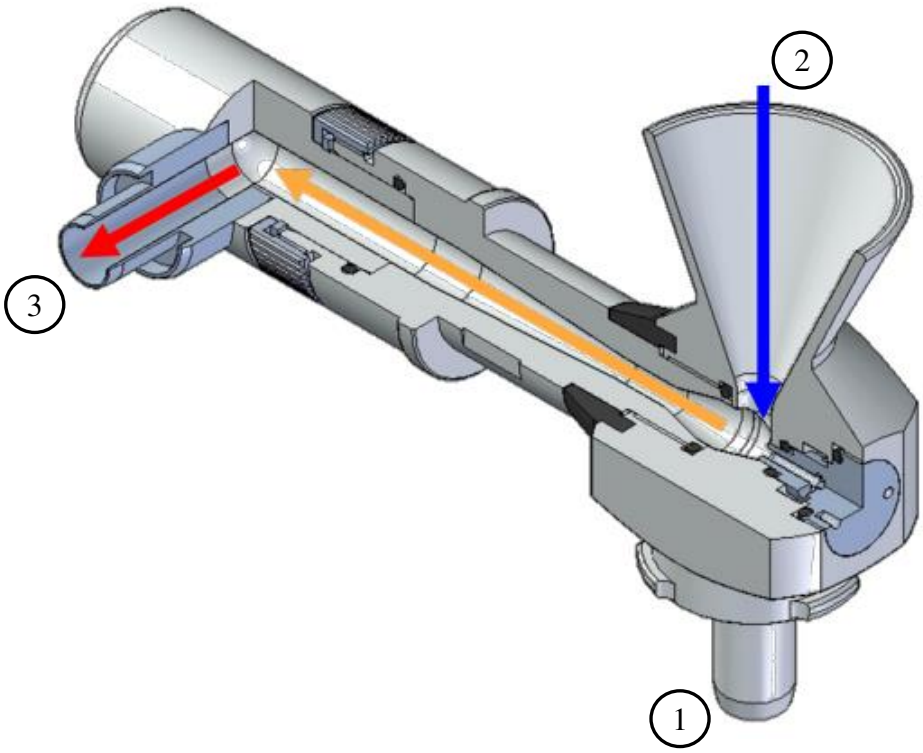

Figure 1 - Aero S disperser with high fluid energy Venturi design (Malvern Pananatical, Malvern, UK)

The present work follows the work of Ali *et al.* (2015) and Bonakdar *et al.* (2016) on the breakability assessment of α-lactose monohydrate (α-LM), aspirin and sucrose in the Scirocco dispersion unit. Paracetamol crystals are additionally tested here. The same methodology is followed here to facilitate comparison. The impact velocities of particles of different sizes are obtained by carrying out numerical analysis of the fluid flow field by Computational Fluid Dynamic modelling and Lagrangian particle tracking to estimate the impact velocity. The impact velocities are used to estimate breakage propensity parameter. The extent of breakage and change in the specific surface area is then related to the breakage propensity parameter.

2. CFD Modelling of Fluid Flow Field and Lagrangian Particle Trajectory Calculation

Three-dimensional multiphase CFD modelling of the disperser is carried out to predict the air flow profiles at different inlet air pressures. The geometry of the disperser was provided by Malvern Panalytical, Malvern, UK. The geometry was imported to Ansys Meshing software to generate three-dimensional mesh of the disperser. A mesh independency study was carried out to ensure that the predicted air flow profiles are mesh independent. The selected mesh

comprises primarily tetrahedral cells. Total number of cells in the computational mesh are 3.8 $\times 10^5$ cells. A cross-sectional view of the selected mesh is depicted in Figure 2.

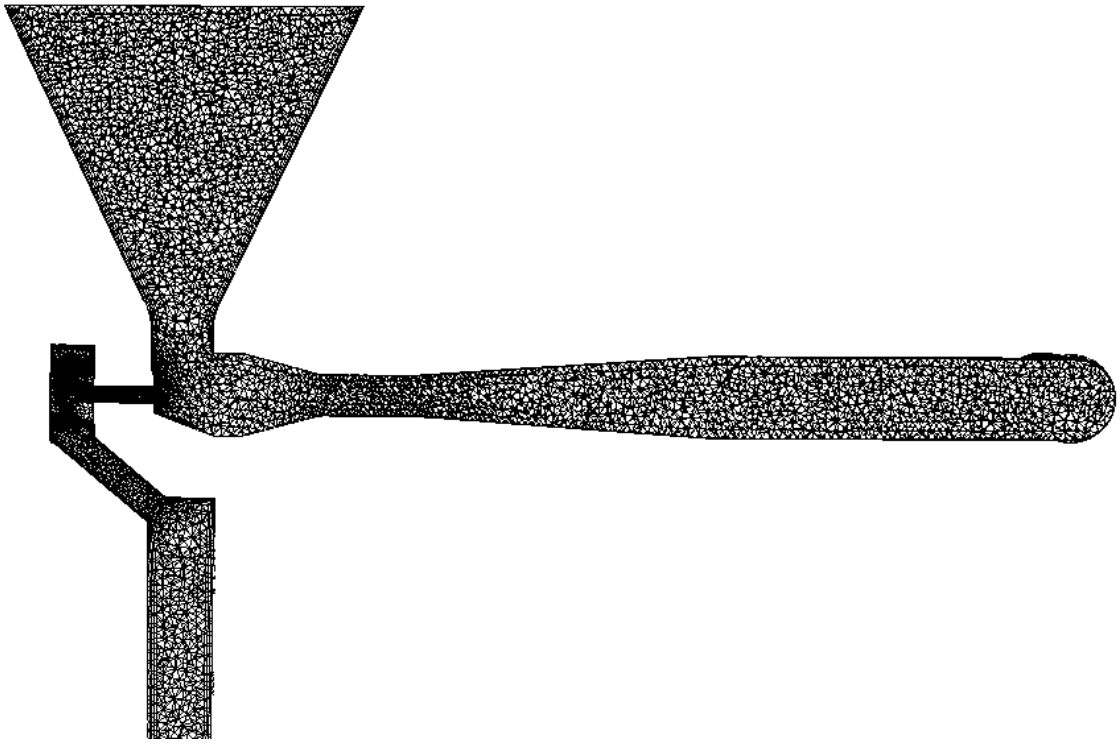

Figure 2 - Cross-sectional view of the mesh used for CFD analysis

The conservation equations for the continuous and discrete phases are solved using commercial CFD software Ansys Fluent v. 16.2 (Ansys, 2016) for compressible flow. Steady-state assumption is used for prediction of the air flow profiles. The turbulence is modelled using the Reynolds Stress Turbulence model. Details of the CFD modelling methodology can be found in Ali *et al.* (2015) and Bonakdar *et al.* (2016). Particles are introduced from port 2 (Figure (1)) and the trajectories are calculated using one-way coupled Eulerian-Lagrangian approach, i.e., the momentum of the particles does not influence the surrounding air flow and particle-particle interactions are ignored. In the equation of motion of particles, drag and gravitational forces are considered. The drag law applicable to smooth spherical particles given by Morsi and Alexander (1972) is considered for calculation of drag coefficient. Particle dispersion due to turbulence is taken into account using the discrete random walk model (Hutchinson *et al.*, 1971). Change in size distribution of particles due to breakage is not considered in the CFD model. The restitution coefficient (ratio between the particle rebound velocity after impacting the wall and the incident particle velocity) is specified to be 0.9 for both tangential and wall-normal components. For each particle size, 250 particles are introduced from the top. The average of the first impact velocity of each particle at the elbow of the

disperser is taken as the impacting particle velocity, which is used in the calculation of breakage propensity.

The influence of inlet pressure on the air flow and the corresponding impact velocities of particles is assessed by varying the inlet air pressure from 0.5 barg to 3 barg pressure with an increment of 0.5 barg. For each case, pressure inlet boundary condition is specified at the inlet port 1 (Figure 1), while pressure outlet boundary condition with atmospheric pressure is specified at ports 2 and 3. Particle sizes in the range of 10 µm to 600 µm are considered. The density of particles is varied from 800 kg/m^3 to 1500 kg/m^3.

3. CFD MODELLING RESULTS

Contours of velocity profile of air obtained using different inlet air pressures are depicted in the Figure 3. The highest velocity occurs at the tip of the nozzle and reduces downstream of the disperser. The maximum velocity of air jet inside the disperser is at the top of the inlet nozzle inside the disperser where the flow is supersonic above 2 barg pressure. The jet velocity reduces as it moves downstream.

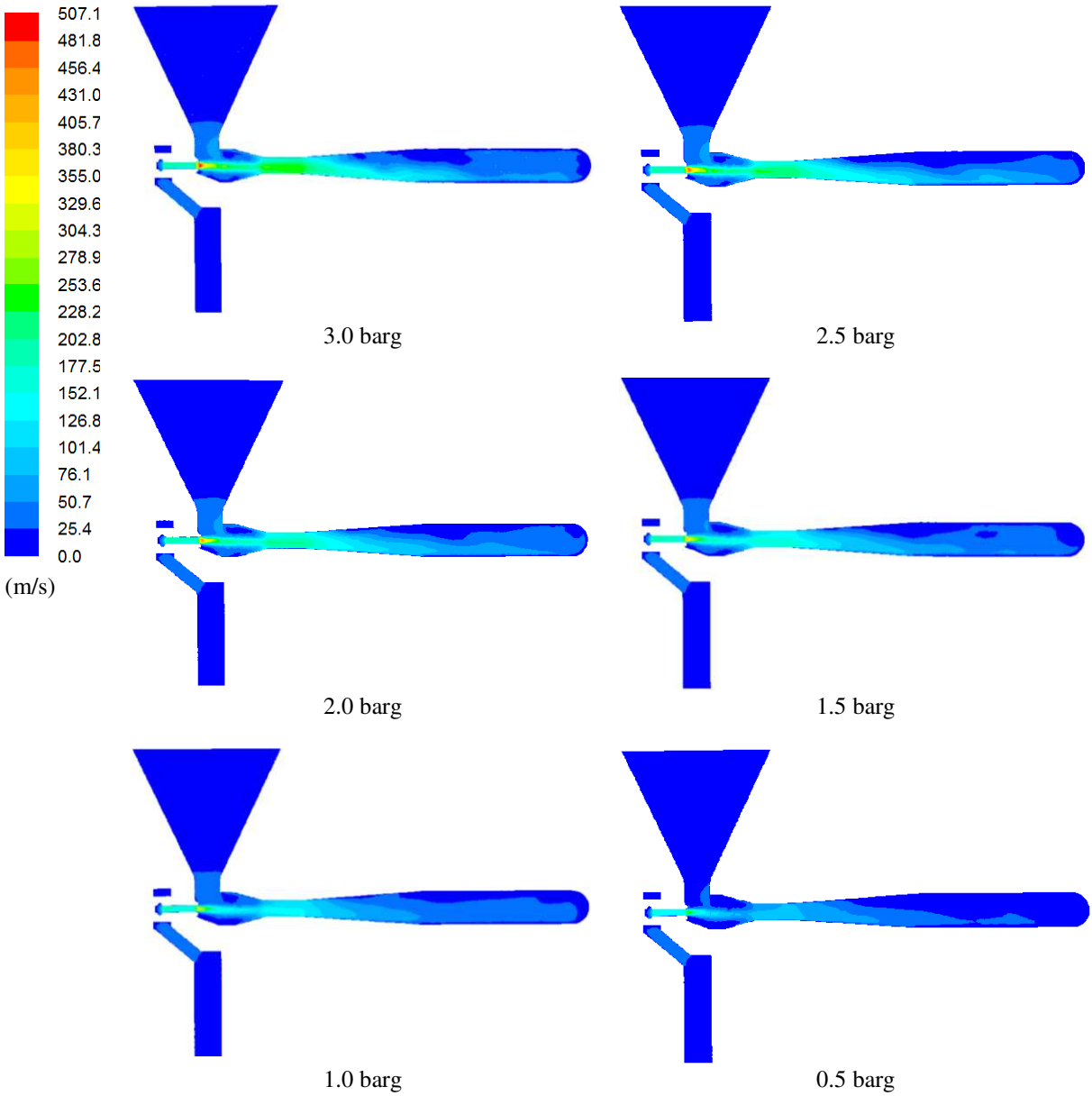

Figure 3 - Contours of velocity profiles of air coloured by velocity magnitude (m/s)

Predicted trajectories of particles at 2.5 barg are depicted in Figure 4, considering the particle density of 1500 kg/m^3. The tracks of particles are coloured by particle velocity magnitude. The particles fall under gravity and then are entrained into the jet stream. . They collide with the surrounding walls in the entrance region with an oblique angle at low impact velocity. They are then accelerated along the length of the horizontal pipe by the air flow and eventually hit the elbow of the disperser. The smaller particles get accelerated to a higher velocity compared to larger particles owing to lower inertia.

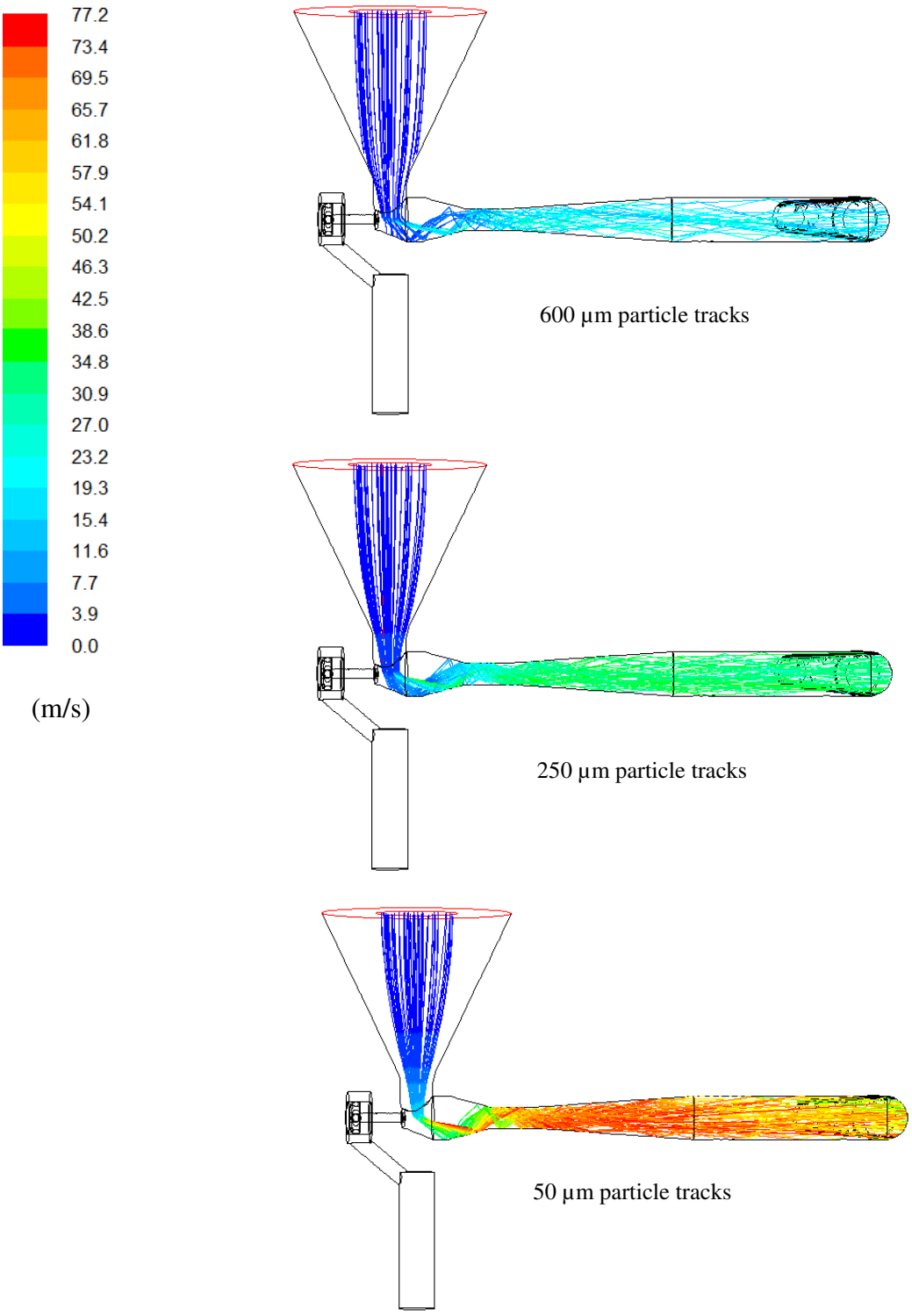

Figure 4 - Predicted trajectories of particles of different sizes at 2.5 barg pressure

The impact velocity of particles at the elbow is calculated by taking the arithmetic average of velocity for 250 particle tracks of each particle size. The effect of the nozzle pressure on the average impact velocity of particles of different sizes is depicted in Figures 5 (a) to (c). In general, the impact velocity of each particle size is found to increase with increasing inlet air pressure. With decreasing the density of particles from 1500 kg/m^3 to 800 kg/m^3, the impact

velocity is found to increase. For each pressure, a general trend of decreasing impact velocity with increasing size is predicted for particles larger than from 50 µm. The trend for smaller particles is erratic as they have low inertia, hence respond faster to the changing air velocity and are more affected by the turbulence, implying a larger number would have been needed to obtain a smoother trend. Moreover, the smaller particles decelerate faster as they approach the elbow where the air flow changes direction, hence the impact velocity of these particles is lower than those larger particles. So an overlap in the impact velocity of particle sizes less than 50 µm is predicted for inlet pressures greater than 1 barg (depending on particle density). Smaller and lighter particles have a shorter response time, which is a measure of how fast the particles respond to changes in the surrounding air velocity. Considering the Stokes regime for example, the particle response time (τ_p) is defined as $\tau_p = \rho_p \, d_p^2/18\mu_{air}$. For example for particles of 50 µm diameter the response is 12×10^{-3}, 9.2×10^{-3} and 6.2×10^{-3} s for densities of 1500, 1200 and 800 kg/m^3, respectively. Larger particles do not accelerate fast enough to high velocities (Figure 4) hence the impact velocity of large particles is also lower than small ones. Particles with sizes in the range of 20 µm to 30 µm exhibit the highest impact velocity. However, much larger particle sizes are used in the experimental work and hence the following analysis uses the data for particle sizes larger than 50 µm.

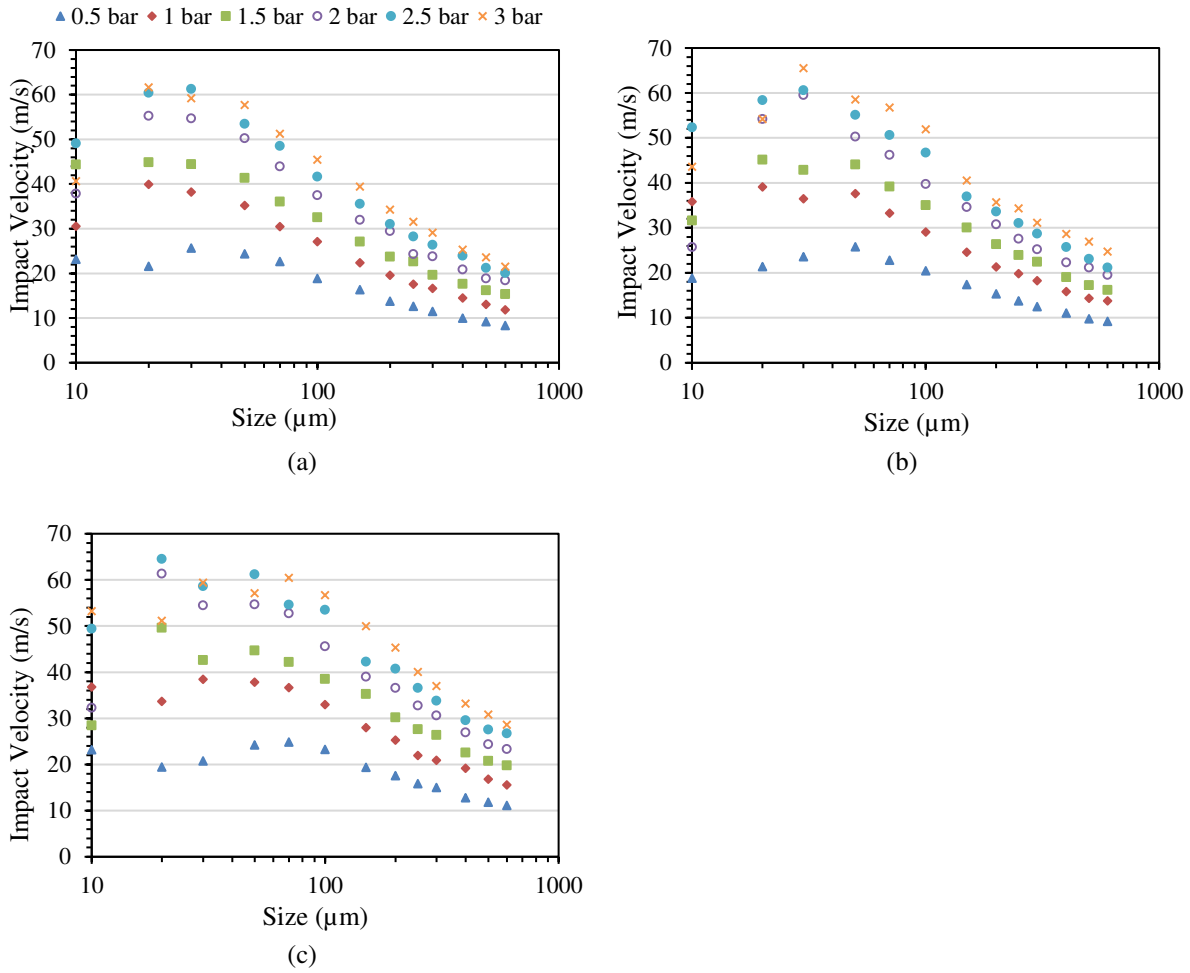

Figure – 5: Semi-logarithmic plot of impact velocity of particles as a function of particle size at different inlet air gauge pressures; a: Particle density of 1500 kg/m^3, b: Particle density of 1200 kg/m^3, c: Particle density of 800 kg/m^3

Empirical Correlation of Particle Impact Velocity

Particle impact velocity is obtained using CFD simulations for the inlet air pressures and particles sizes as shown in Figure 5 and for three particle densities, i.e. 800 kg/m^3, 1200 kg/m^3 and 1500 kg/m^3. Based on these data, an empirical correlation is proposed heuristically following the form of numerous empirical formulae available in literature for particle terminal velocity as a function of particle size and density and the fluid properties in non-dimensional form, as given by equation (1):

$$N_v^{1/3} = 0.02\left[\frac{\left(\frac{P}{\rho_{air} g h}\right)^{0.9}}{(S-1)^{0.4}\left(N_d\right)^{\frac{0.4}{3}}}\right] \tag{1}$$

where N_v is the dimensionless impact velocity, P is the inlet pressure of the disperser in Pa (absolute), ρ_{air} is the inlet air density (kg/m^3), g is the acceleration due to gravity (m/s^2), h is the length from nozzle tip to impact elbow (0.09 m). N_v is given by:

$$N_v^{1/3} = v_p\left[\frac{3}{4\,g\,\gamma\,(S-1)}\right]^{1/3} \tag{2}$$

N_d in equation (1) is the dimensionless particle size given by:

$$N_d^{1/3} = d_p\left[\frac{4\,g\,(S-1)}{3\gamma^2}\right]^{1/3} \tag{3}$$

where d_p in equation (3) is particle diameter in m.

S in equations (2) and (3) is given by:

$$S = \frac{\rho_p}{\rho_{air}} \tag{4}$$

where ρ_p in the above equation is the density of the material in kg/m^3. γ in equations (2) and (3) is given by:

$$\gamma = \frac{\mu_{air}}{\rho_{air}} \tag{5}$$

Equation (1) has been developed for particle sizes ranging from 50 µm to 600 µm and for materials having density ranging from 800 to 1500 kg/m^3, using CFD data for inlet air pressures ranging from 0.5 barg to 3.0 barg. A comparison between the CFD-based calculated

values and those predicted by equation (1) is given in Figure 6 for particle density of 1500 kg/m^3. The dashed lines represent the predicted N_v calculated using equation (1). The maximum difference between the CFD-determined N_v and correlation is within 12% error. It should be noted that the correlation is not valid for particles smaller than 50 µm.

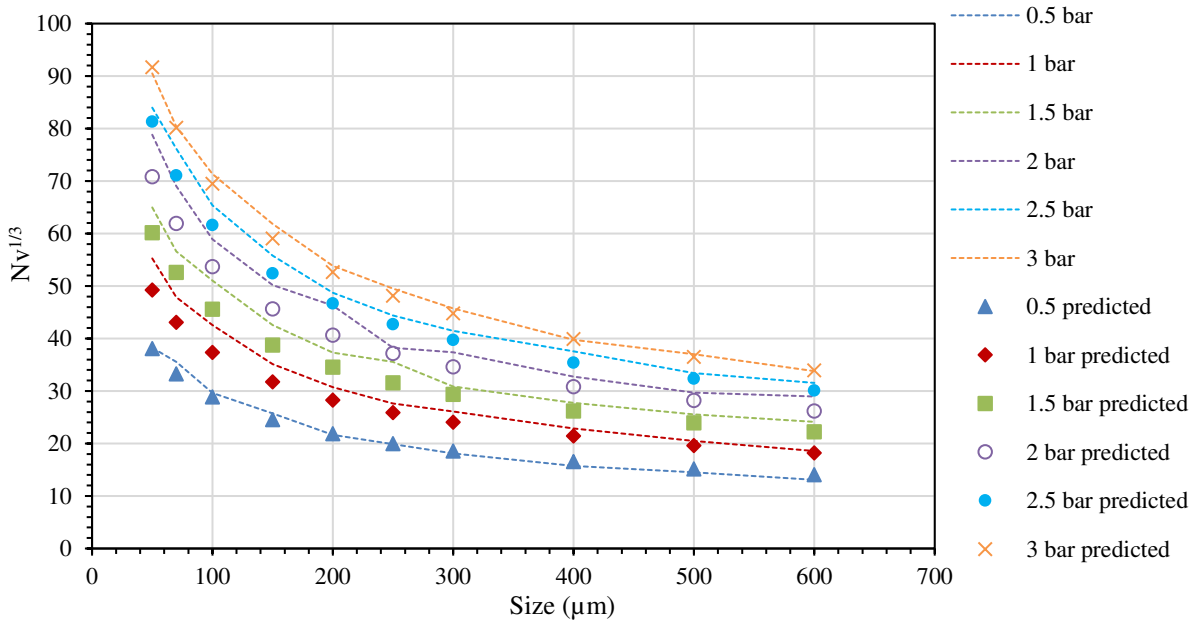

Figure 6 - Comparison between CFD based (solid lines) and estimated N_v values (dotted points) for different gauge pressures for particles having density of 1500 kg/m^3

4. EXPERIMENTAL METHOD

Crystals of aspirin, sucrose, paracetamol and α-lactose monohydrate (α-LM) have been used as test materials . Crystals of α-LM were donated by DFE Pharma (DFE Pharma GmbH & Co. KG, Goch, Germany) and crystals of other test materials were purchased from Sigma–Aldrich, UK. The material batches used for this study are the same as those used in the work of Bonakdar et al. (2016). This provides a common ground to compare the particle breakage in the Aero S disperser of Malvern Mastersizer 3000 with the Scirocco disperser of Mastersizer 2000. Each material is sieved using a number of sieve cuts in order to generate narrow sieve sizes of each material. Sieve sizes 212-250 µm, 355-425 µm and 500-600 µm for aspirin, 355-425 µm, 500-600 µm and 710-850 µm for sucrose, 355-425 µm, 425-500 µm and 500-600 µm for paracetamol and 125-140 µm, 160-180 µm and 212-250 µm for α-LM have been used in this study. Each sieve cut is then fed into the Aero S (high energy disperser) of Malvern Mastersizer 3000. The feed rate is set to provide an acceptable obscuration range for the measurements. Each sieve size is tested using air pressure conditions: 0.5, 1, 1.5, 2, 2.5, 3, 3.5 and 4 barg. CFD simulation has been used to estimate the impact velocity of different sizes of each material at the L-bend of the disperser, using the equations of Section 3. The particle

densities used for the calculation of impact velocities are 1397, 1290, 1590 and 1520 kg/m^3 for aspirin, paracetamol, sucrose and α-LM, respectively.

5. EXPERIMENTAL RESULTS AND DISCUSSION

Malvern Mastersizer software reports the particle size distributions of the test materials for each test conditions. It also reports $d_{3,2}$ of the distribution, by which the specific surface area (SSA) of the particles is calculated. The size distribution and specific surface area (SSA_0) of feed particles have been obtained by running the test at 0.1 barg air pressure, where little/no damage is imparted to the particles. The information on particle size distribution and density, and impact velocity are then used to calculate the extent of breakage of the three sieve cut sizes of each material. The volumetric average size, $d_{4,3}$ obtained by laser diffraction technique at 0.1 barg has been used as an average feed particle size for impact velocity calculations.

Particles of different sizes impact at different impact velocities. Therefore, it is important to use as narrow particle size distribution as possible. Particles of each sieve cut size are then placed on the vibratory feeder of the Aero S disperser. Approximately 1-2 g of each sample has been used to carry out the tests at each condition. Sensitivity analysis has been carried out to find the right feeding rate to provide an acceptable obscuration range. The measurements which do not fall into this range are discarded. Particle size distribution at each test condition is then obtained. The size distributions of 212-250 µm particles of aspirin at different air pressures are shown in the Figure 7(a) as an example. Probability density function (normalised frequency% based on the particle bin size) with the logarithmic x-axis is also shown in Figure 7(b), as it visualises better the fine tale of the distribution.

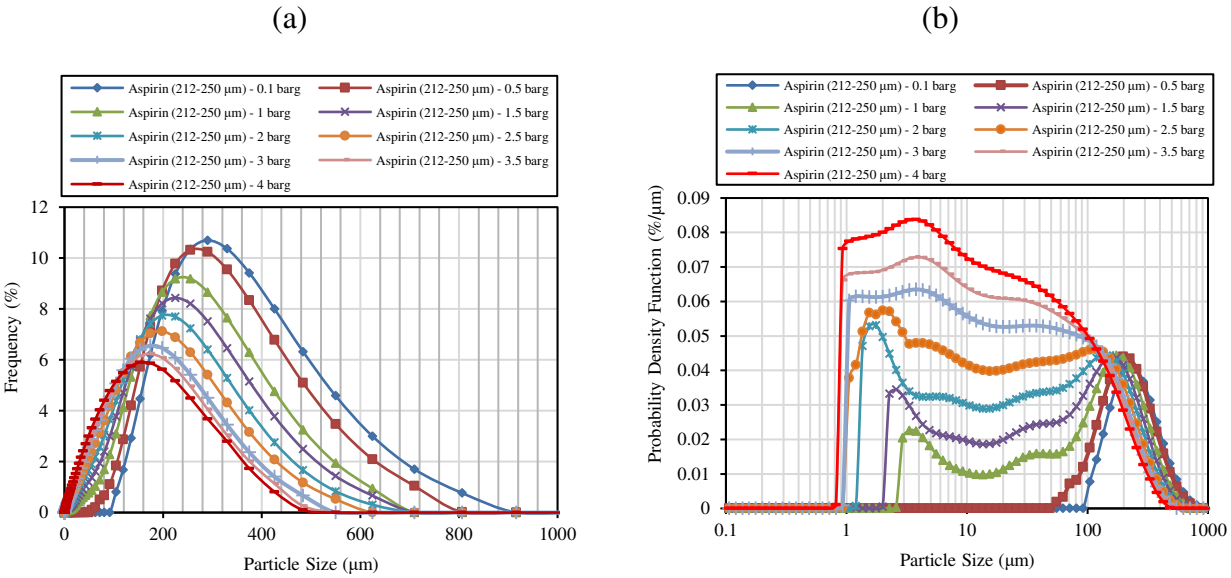

Figure 7- Particle size distribution (a) and probability density function (b) of 212-250 µm aspirin particles at different nozzle air pressures using Aero S of Malvern Mastersizer 3000

The size distribution of the feed particles of 212-250 µm of aspirin (at 0.1 barg) shows a mono modal size distribution (see Figure 7). As a result of increase in the nozzle air pressure from 0.1 to 0.5 barg, there is a slight shift in the particle size distribution to the left, indicating breakage of particles. A further increase in the nozzle air pressure results in producing fine particles and generating bi-modal distribution. This can be clearly observed in Figure 7(b).

Characteristic measures of the size distributions of broken particles of the test materials, d_{10}, d_{50} and d_{90} at nozzle pressures of 0.1, 1, 2, 3 and 4 barg are listed in Tables 1-4 for aspirin, paracetamol, sucrose and α-LM, respectively.

Table 1 – d_{10}, d_{50} and d_{90} of the size distributions of broken aspirin particles obtained by operating Aero S using different air pressures

Material	Aspirin								
Feed particle size	212-250 µm feed size			355-425 µm feed size			500-600 µm feed size		
Pressure	d_{10} (µm)	d_{50} (µm)	d_{90} (µm)	d_{10} (µm)	d_{50} (µm)	d_{90} (µm)	d_{10} (µm)	d_{50} (µm)	d_{90} (µm)
0.1 barg	158	289	517	247	453	812	278	539	986
1 barg	85	217	409	149	347	679	156	389	785
2 barg	41	167	348	67	249	540	77	292	642
3 barg	24	125	292	40	199	459	42	218	528
4 barg	18	107	280	29	165	391	33	189	476

Table 2- d_{10}, d_{50} and d_{90} of the size distributions of broken paracetamol particles obtained by operating Aero S using different air pressures

Material	Paracetamol								
Feed particle size	425-500 µm			600-710 µm			710-850 µm		
Pressure	d_{10} (µm)	d_{50} (µm)	d_{90} (µm)	d_{10} (µm)	d_{50} (µm)	d_{90} (µm)	d_{10} (µm)	d_{50} (µm)	d_{90} (µm)
0.1 barg	335	499	741	532	755	1060	589	837	1190
1 barg	81.5	339	615	140	501	912	178	586	1060
2 barg	33.2	248	542	56.2	366	782	68.6	409	862
3 barg	20.4	192	482	34.1	280	666	40.3	327	801
4 barg	16.3	162	448	25.3	240	635	28.6	268	713

Table 3- d_{10}, d_{50} and d_{90} of the size distributions of broken sucrose particles obtained by operating Aero S using different air pressures

Material	Sucrose								
Feed particle size	355-425 µm feed size			500-600 µm feed size			710-850 µm feed size		
Pressure	d_{10} (µm)	d_{50} (µm)	d_{90} (µm)	d_{10} (µm)	d_{50} (µm)	d_{90} (µm)	d_{10} (µm)	d_{50} (µm)	d_{90} (µm)
0.1 barg	359	481	646	496	659	875	685	896	1180
1 barg	275	433	646	404	609	894	598	879	1350
2 barg	156	366	617	254	536	894	397	787	1370
3 barg	79.8	300	544	122	429	787	187	626	1150
4 barg	62.1	262	513	93.3	374	730	138	537	1050

Table 4- d_{10}, d_{50} and d_{90} of the size distributions of broken α-lactose monohydrate particles obtained by operating Aero S using different air pressures

Material	α-Lactose Monohydrate								
Feed particle size	124-140 µm feed size			160-180 µm feed size			212-250 µm feed size		
Pressure	d_{10} (µm)	d_{50} (µm)	d_{90} (µm)	d_{10} (µm)	d_{50} (µm)	d_{90} (µm)	d_{10} (µm)	d_{50} (µm)	d_{90} (µm)
0.1 barg	42.1	92.7	158	48.2	104	180	48.7	133	240
1 barg	33.9	88.5	153	40.5	99.7	175	40.9	125	232
2 barg	25.2	82.8	147	29.6	92.4	167	31.8	116	222
3 barg	21.5	79	157	22.8	85	161	25.9	106	213
4 barg	17.9	72.2	136	20.8	81.5	157	23.6	101	208

Based on the CFD calculation results, the first impact on the L-bend is the highest, and hence responsible for breakage. The specific surface area of the particles after impact at different dispersion conditions is reported by Malvern Mastersizer 3000 software. Changes in the specific surface area of the particles as a result of impact are indicative of breakage. Therefore the relative shift in the specific surface area is calculated by normalising the change in the specific surface area of the particles due to breakage, ΔSSA, (i.e. the difference between the specific surface area of impacted particles and that of feed particles) by the feed surface

area (ΔSSA_0). The test particles, having gone the disperser and laser diffraction instrument are then collected using a cyclone.

In order to quantitatively assess the extent of particle breakage in Aero S at different test conditions, a theory/model is needed. Bonakdar et al. (2016) previously developed a breakage model, based on the model of Ghadiri and Zhang (2002), to quantify the extent of breakage in the Scirocco disperser of Malvern Mastersizer 2000. The same approach is adopted here and the same materials are used to enable a comparison to be made. The breakage model expresses the relative shift in the specific surface area of the particles, $\frac{\Delta SSA}{SSA_0}$, as a function of feed and broken particles properties, as well as the impact velocity of the particles in the Aero S, V, calculated by CFD simulation. The breakage model is shown below, in Eq. (6).

$$\frac{\Delta SSA}{SSA_0} = \beta \frac{\rho_f \bar{d}_{f,v} V^2 H}{K_c^2} \times \frac{\rho_f \bar{d}_{f,v}}{\rho_d \bar{d}_{d,v}} \qquad (6)$$

where ρ_f and ρ_d are the densities of feed and broken particles, respectively. H is the material hardness, K_c is the fracture toughness and β is the proportionality constant, obtained by linear regression. $\bar{d}_{f,v}$ and $\bar{d}_{d,v}$ represent average size (volumetric base) of feed particles and the average size of debris produced as a result of impact breakage, respectively. The details of $\bar{d}_{d,v}$ calculation, using the particle size distribution results, have been described in the work of Bonakdar et al. (2016). For non-porous materials and solid crystalline structures the envelope density of the particles remains the same after breakage. This is also the case for the materials used in this study. Plotting $\frac{\Delta SSA}{SSA_0}$ as a function of $\rho_f \bar{d}_{f,v} V^2 \frac{\bar{d}_{f,v}}{\bar{d}_{d,v}}$ for all the tests, the slope of the line is $\beta \frac{H}{K_c^2}$, which gives an indication of breakability based on Eq. (6); the larger the slope the easier the particles break. The breakability indices (slope of the lines) of the test materials obtained from Aero S of Malvern Mastersizer 3000 are listed in Table 5.

Table 5- Slope of the lines for the test materials obtained by Aero S

Material	Slope ($\beta \frac{H}{K_c^2}$)
Aspirin	0.0031
Sucrose	0.0018
Paracetamol	0.0063
α-LM	0.0006

In order to validate the approach, the ratio of the slopes of each two test materials is compared to those obtained by the Scirocco disperser of Malvern Mastersizer 2000 and single particle impact test, as previously given by Bonakdar et al. (2016). This is shown in Table 6; despite the differences between the ratios obtained by the three techniques, the ratios for aspirin-sucrose and paracetamol-aspirin are comparable. However, for α-LM there is a significant difference between the ratios obtained by Aero S of Malvern Mastersizer 3000 and those of single particle impact testing and Scirocco disperser. α-LM has a high surface energy and is known to attract fine debris to its surfaces. Previous studies by Bentham et al. (1997) and Dogbe (2017) showed the presence of very fine (sub 50 µm) particles adhered to the surfaces of the larger lactose particles. Therefore it was decided to wash lactose particles in order to eliminate the effect of the surface dust on the breakage results in Aero S. This also provides consistency with the work of Bonakdar et al. (2016), for which washed α-LM had been used for both single particle impact testing and Scirocco tests. The washing process was carried out by placing sieve cut sizes of 125-140 µm, 140-160 µm and 160-180 µm of lactose on a small sieve cut (45 µm) and rinsing them with propan-2-ol. A notable amount of debris was washed out by this process. Sieves were then placed on top of a base tray, and left at the room temperature for 72 hours, with the sieve surfaces covered with a cloth, in order to protect the material from dust. Once dried, the materials were tested and analysed again following the same approach. The results are shown in Figure 8, where $\frac{\Delta SSA}{SSA_0}$ is plotted as a function of $\rho_f \bar{d}_{f,v} V^2 \frac{\bar{d}_{f,v}}{\bar{d}_{d,v}}$ and compared with the results of the other test materials. Washing α- LM has made a significant difference in its breakability index. The slope of the line has changed from 0.0006 to 0.001. As shown in Figure 8, the results for paracetamol show some non-linearity in the data trend, likely due to the method used in the calculation of the surface area, meriting further probing in examining the underlying mechanism.

Table 6- Ratio of the slopes for each two materials obtained by impact testing, Scirocco disperser and Aero S disperser

Material	Ratio of slopes (Impact testing)	Ratio of slopes (Scirocco tests)	Ratio of slopes (Aero S tests)
Aspirin/Sucrose	1.9	2.0	1.7
Sucrose/α-LM	1.5	1.5	3.0
Aspirin/α-LM	2.9	3.0	5.1
Paracetamol/Aspirin	1.6	1.6	2.0

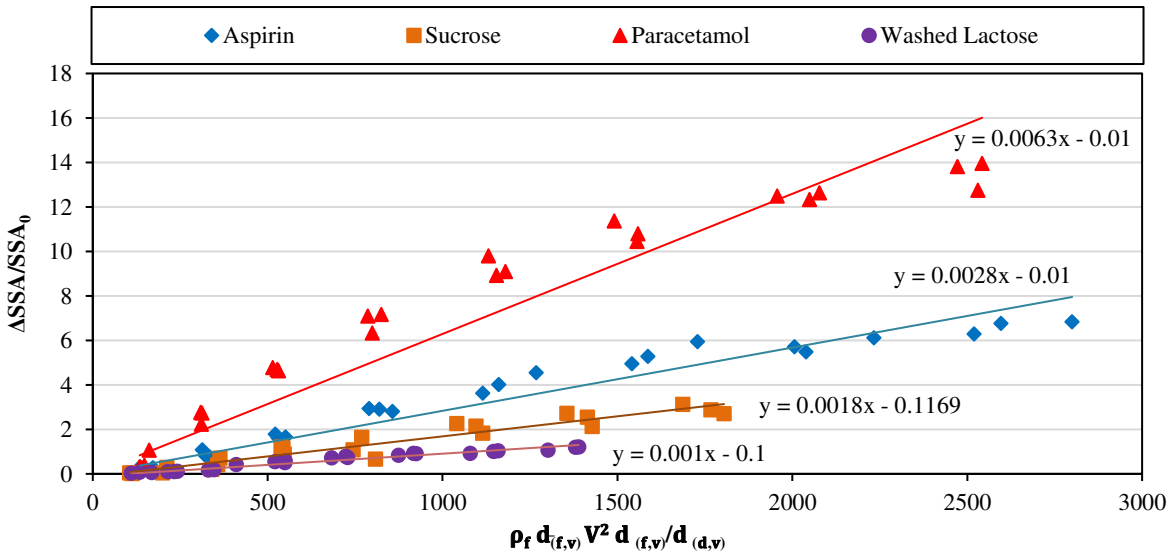

Figure 8- $\frac{\Delta SSA}{SSA_0}$ as a function of $\rho_f \bar{d}_{f,v} V^2 \frac{\bar{d}_{f,v}}{\bar{d}_{d,v}}$ obtained from Aero S of Malvern Mastersizer for different materials

In order to provide a better understanding of the effect of washing on the breakage results of α-LM, $d_{3,2}$ of 160-180 µm feed particles have been exported and listed in Table 7. The $d_{3,2}$ of unwashed lactose is always smaller than that of washed particles for the same test condition. The reason is that the dust on the surfaces of the unwashed particles contributes to the fine portion of the broken particles, and therefore a smaller surface mean diameter is reported for the unwashed particles by Aero S. However, as the dust on the surface comes off after washing, the only fine particles in the distribution are produced as a result of breakage. Therefore, the Aero S data using unwashed lactose do not represent the real breakage behaviour

of the particles in the disperser, and the washed lactose data have been used for final analysis. The data of Table 6 are then updated using the new slope of washed lactose data. The new ratios of the slopes of each two materials are shown in Table 8.

Table 7- Comparison between $d_{3,2}$ of washed and unwashed lactose particles at different test conditions of Aero S

	160-180 µm Sieve Cut of α-LM	
$d_{3,2}$ (µm) at Different Test Conditions	**Unwashed**	**Washed**
0.1 barg	62.5	91.9
0.5 barg	56.7	86.5
1 barg	50.1	83.5
1.5 barg	45.7	77.5
2 barg	45.6	61.1
2.5 barg	41.6	53.1
3 barg	38.7	48.3

Table 8- Ratio of the slopes for each two materials obtained by impact testing, Scirocco disperser and Aero S disperser (using washed α-LM data)

Material	Ratio of slopes (Impact testing)	Ratio of slopes (Scirocco tests)	Ratio of slopes (Aero S tests)
Aspirin/Sucrose	1.9	2.0	1.7
Sucrose/α-LM	1.5	1.5	1.8
Aspirin/α-LM	2.9	3.0	3.1
Paracetamol/Aspirin	1.6	1.6	2.0

Using the data of washed lactose, a good agreement is observed between different techniques. Despite particles having different sizes and impacting at different velocities, making use of the estimated particle impact velocity in the Aero S disperser, average size of debris produced and properties of the material leads to unification of the data. The agreement in the ratio of slopes obtained by three different techniques, single particle impact tester, Scirocco disperser of Malvern Mastersizer 2000 and Aero S of Malvern Mastersizer 3000 also shows that all techniques are capable of providing a comparison between ease of breakability of different materials. Using a small sample quantity, short duration of the test and availability of the device are advantageous for evaluating the breakability of the materials. The information

obtained in this way can be used to predict the milling behaviour of the material in mill types, in which mechanical stressing is due to impact (Bonakdar and Ghadiri, 2018).

6. CONCLUSIONS

Particle breakage due to impact in the Aero S disperser of Malvern Mastersizer 3000 has been evaluated through an integrated experimental and modelling approach. Different sieve cuts of aspirin, sucrose, paracetamol and α-LM have been used as the test materials. The relative shift in the specific surface area of the particles is determined by particle size analysis and used to deduce the ease with which particles could break. For this purpose the particle impact velocity on the right-angle bend of the disperser is estimated using one-way Eulerian-Lagrangian CFD simulation. Based on this, an empirical correlation is proposed for the impact velocity, accounting for particle size and density and disperser nozzle pressure. The particle impact velocity is then used together with the feed particle physical and mechanical properties in a semi-brittle model of impact breakage to describe the relative shift in the specific surface area of the particles (representative of the extent of breakage). A good fit is obtained by linear regression. The slope of the fitted line gives an index of impact breakability, showing paracetamol to be the easiest material to break, followed by aspirin, sucrose and α-LM.

The ratio of the breakability indices of each two test materials is then compared to those obtained by the Scirocco disperser unit of Malvern Mastersizer 2000 and by the single particle impact tester. A good agreement is obtained between these techniques, implying the particle breakage in the Aero S disperser can be used to deduce the breakability index. In the first instance such information is useful to establish a bench mark for relative breakability of different materials. In the longer term, the approach can be used in modelling of various milling devices to provide a predictive tool for milling based on using a very small quantity of the materials.

ACKNOWLEDGEMENT

The authors would like to thank Dr Paul Kippax, Malvern Panalytical Ltd, Malvern, UK, for providing information on the design of Aero S disperser for CFD calculations, and also Dr Bastiaan Dickhoff, DFE Pharma, Goch, Germany, for providing α-lactose monohydrate crystals. The research related to this article did not receive any specific grant from funding agencies in the public, commercial, or not-for-profit sectors.

REFERENCES

Ali, M., Bonakdar, T., Ghadiri, M., Tinke, A., 2015. Particle breakage in a Scirocco disperser. Powder Technol., 285, 138-145.

Ansys. 2016. ANSYS® Academic Research, Release 16.2.

Bentham, A. C., Arteaga, P. A. And Ghadiri, M., 1997. Impact breakage of pharmaceutical powders. In Proc. 1st European Conf. Chemical Engineering, Florence, May 4-7, 2, 887-890.

Bonakdar, T., Ali, M., Dogbe, S. and Ghadiri, M. and Tinke, A., 2016. A method of grindability testing using the Scirocco disperser. Int. J. Pharm., 501, 65-74.

Bonakdar, T. and Ghadiri, M., 2018. Analysis of pin milling of pharmaceutical materials. Int. J. Pharm., 552(1-2), 394-400.

Calvert, G., Ghadiri, M. and Tweedie, R., 2009. Aerodynamic dispersion of cohesive powders: a review of understanding and technology, Adv. Powder Technol. 20, 4-16.

Chaudhri, M.M., Wells, J.K. and Stephens, A., 1980. Dynamic hardness, deformation and fracture of simple ionic crystals at very high rates of strain, Philosophical Magazine A, 43(3), 643-664.

Dogbe, S.C., 2016. Predictive Milling of Active Pharmaceutical Ingredients and Excipients. Doctoral dissertation, University of Leeds.

Fulchini, F., Nan, W., Ghadiri, M., Yazdanpanah, M., Bertholin, S., Amblard, B., Cloupet, A. and Gauthier, T., 2017. CFD-DEM Analysis of Particle Attrition in a Jet in a Fluidised Bed. In EPJ Web of Conferences.140, 07017. EDP Sciences.

Ghadiri, M. and Zhang, Z., 2002. Impact attrition of particulate solids. Part 1: A theoretical model of chipping. Chem. Eng. Sci. 57(17), 3659-3669.

Ghadiri, M., Pasha, M. and Zafar, U., 2020. Hardness, stiffness and toughness of particles. Chapter 1.5, Powder Technology Handbook 4th Edition, Eds: K. Higashitani, H. Makino, and S. Matsusaka, CRC Press, 33-40.

Gong, D., Nadolski, S., Sun, C., Klein, B. and Kou, J., 2018. The effect of Strain Rate on Particle Breakage Characteristics. Powder Technol. 339, 595-605.

Hebbink, G.A. and Dickhoff, B.H., 2019. Application of lactose in the pharmaceutical industry. In Lactose. 175-229. Academic Press.

Hutchinson, P., Hewitt, G. F., Dukler, A. E., 1971. Deposition of liquid or solid dispersions from turbulent gas streams: A stochastic model. Chem. Eng. Sci. 26, 419-439.

Kwade, A. and Schwedes, J., 2002. Breaking characteristics of different materials and their effect on stress intensity and stress number in stirred media mills, Powder Technol. 122, 109-121.

Lecoq, O., Chamayou, A., Dodds, J. A., and Guigon, P., 2011. Application of a simplifying model to the breakage of different materials in an air jet mill. Int. J. Miner. Processes. 99 (1–4), 11-16.

Lecoq, O., Chouteau, N., Mebtoul, M., Large, J. F., and Guigon, P., 2003. Fragmentation by high velocity impact on a target: a material grindability test. Powder Technol, Volume 133 (1–3), 113-124.

Meier, M., John, E., Wieckhusen, D., Wirth, W., and Peukert, W., 2008. Characterization of the grinding behaviour in a single particle impact device: studies on pharmaceutical powders. Eur J Pharm Sci. Volume 34 (1), 45-55.

Meier, M., John, E., Wieckhusen, D., Wirth, W., and Peukert, W., 2009. Influence of mechanical properties on impact fracture: Prediction of the milling behaviour of pharmaceutical powders by nanoindentation. Powder Technol., 188, 301-313.

Morsi, S. A. and Alexander, A. J., 1972. An investigation of particle trajectories in two-phase flow systems. J. Fluid Mech., 55, 193-208.

Olusanmi, D., Roberts, K.J., Ghadiri, M., Ding, Y., 2011. The breakage behaviour of Aspirin under quasi-static indentation and single particle impact loading: Effect of crystallographic anisotropy. Int. J. Pharm. 411 (1–2), 49-63.

Petukhov, Y. and Kalman, H., 2003. A new apparatus for particle impact tests. Particle & Particle Systems Characterization: Measurement and Description of Particle Properties and Behaviour in Powders and Other Disperse Systems, 20(4), 267-275.

Petukhov, Y., and Kalman, H., 2004. Empirical Breakage Ratio of Particles due to Impact. Powder Technol, 143-144, 160-169.

Saeidi, F., Yahyaei, M., Powell, M., and Tavares, M., 2017. Investigating the effect of applied strain rate in a single breakage event. Miner. Eng. 100, 211-222.

Salman, A. D., Biggs, C. A., Fu, J., Angyal, I., Szabo, M., and Hounslow, M. J., 2002. An experimental investigation of particle fragmentation using single particle impact studies. Powder Technol. 128, Issue 1, 4, 36-46.

Salman, A.D., Reynolds, G.K., Fu, J.S., Cheong, Y.S., Biggs, C.A., Adams, M.J., Gorham, D.A., Lukenics, J. and Hounslow, M.J., 2004. Descriptive classification of the impact failure modes of spherical particles. Powder Technol. 143, 19-30.

Schönert, K., and Marktscheffel, M., 1986. Liberation of composite particles by single particle compression, shear and impact loading, 6th European Symposium Comminution, Nürnberg, NMA Nürnberger Messe- u, Ausstellungsges., Nürnberg, 29-45.

Shipway, P.H. and Hutchings, I.M., 1993, Attrition of brittle spheres by fracture under compression and impact loading. Powder Technol. 76, 23.

Tavares, L. M., King, R.P., 1998. Single-particle fracture under impact loading. Int. J. Miner. Process., 54 , 1-28.

Vogel, L., and Peukert, W., 2003. Breakage behaviour of different materials—construction of a master curve for the breakage probability. Powder Technology, 129 (1–3), 101-110

Weichert, R., Herbst, J.A., (1986). An ultrafast load cell device for measuring particle breakage. Prepr. 1st World Congr. Particle Technology, Nürnberg II, 3.

Yüregir, K. R., Ghadiri, M. Clift, R., 1986. Observations on impact attrition of granular solids. Powder Technol., 49, 53-57.